Structural and Multidisciplinary Optimization (2020) 62:2995–3007
https://doi.org/10.1007/s00158-020-02643-y

RESEARCH PAPER

Parametric optimization for morphing structures design: application to morphing wings adapting to changing flight conditions

Jonathan M. Weaver-Rosen[1] · Pedro B. C. Leal[2] · Darren J. Hartl[2] · Richard J. Malak Jr.[1]

Received: 23 January 2020 / Revised: 28 April 2020 / Accepted: 2 June 2020 / Published online: 16 July 2020

Abstract

Morphing structures can allow significant improvements in performance by optimally changing shape across varying conditions. A critical barrier to the design of morphing structures is the challenge of determining how optimal shape changes as a function of the many operating conditions that affect optimality. Traditional engineering optimization techniques are able to determine an optimal shape only for one condition or an aggregation over operating conditions (i.e., optimizing average performance). Parametric optimization is an alternative approach that can solve a family of related optimization problems simultaneously. Herein the authors analyze the design of a structurally consistent camber morphing wing for light aircraft applications using parametric optimization techniques. The approach combines rigorous consideration of structural constraints via Class/Shape Transformation (CST) equations and use of a C^1-continuous analytical representation of wing outer mold line geometry with the Predictive Parametric Pareto Genetic Algorithm (P3GA), an algorithm for nonlinear multi-parametric optimization. The system is tuned to maximize lift-to-drag ratio, a key metric for aircraft flight range. Kriging-based interpolation is applied to P3GA output to obtain an optimal solution map determining optimal shape variable values as a function of flight conditions (airspeed, angle of attack, and altitude). Solutions obtained from iterated use of traditional optimization techniques are utilized to benchmark the more novel and efficient parametric optimization accuracy. Results show that parametric optimization is useful for optimizing morphing structures across a range of operating conditions.

Keywords Parametric optimization · Multi-parametric · Camber morphing · Morphing wing · Design

1 Introduction

The design advantage of morphing structures is that as operating conditions change, the structure can adapt to be optimal in a range of operating regimes as illustrated in Fig. 1. It is possible to optimize a non-morphing structure for average performance over a distribution of potential operating conditions (Fig. 1a), but this still results in suboptimal solutions at any one operating condition. Traditional (non-morphing) structures may be optimized to a specific operating condition, but changes in the external conditions will lead to sub-optimal off-condition performance (Fig. 1b). In contrast, a morphing structure can adapt its geometry to be optimal at any operating condition within some prescribed range.

Successful design of optimally morphing structures requires an advanced technique in engineering optimization. Parametric optimization, also called parametric programming, is a methodology to solve an optimization problem as a function of one or more exogenous parameters (Fiacco 1976). The exogenous parameters are variables that affect optimization results but that are not determined by the optimization process. In an aerospace context, parameter variables can include flight conditions that affect aircraft performance, such as airspeed, angle of attack, and altitude. The underlying concept of using parametric optimization for optimal morphing is the central idea that parameter values could be sensed during system operation and that the system can morph to the solution optimal for the sensed conditions.

Responsible editor: Axel Schumacher

✉ Richard J. Malak Jr.
rmalak@tamu.edu

Extended author information available on the last page of the article.

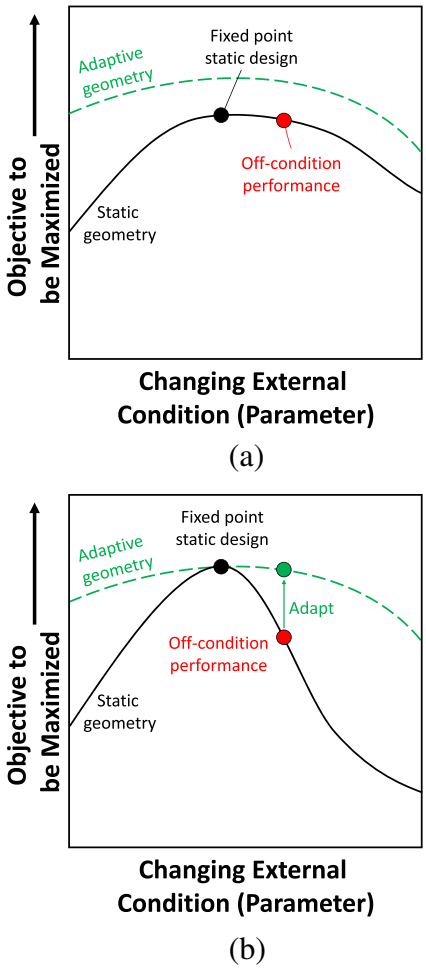

Fig. 1 **a** Static robust design provides less sensitivity to changing conditions but accepts sub-optimality. **b** Morphing designs can adapt to changing conditions to maintain optimality

Engineering researchers have applied parametric optimization in the design of strategies for chemical process control that adapt to changing operating conditions (e.g., plant state (Pistikopoulos et al. 2004), time (Wang et al. 2000), or material availability (Acevedo and Salgueiro 2003) and the design of multifunctional structures in which design requirements are treated as parameters due to their potential to change during the course of a project (Hartl et al. 2016). Parametric optimization also arises in economic analysis called comparative statics, which seeks to identify how market equilibria shift due to changes in exogenous parameters (Spiegel and Subrahmanyam 2015).

To be efficient, parametric optimization requires specialized optimization codes. Although it is possible to iterate a traditional optimization algorithm at different values for parameters, this approach does not scale well. Gamboa et al. (2009) apply such a sampling approach to the parametric optimization of a morphing wing, but deals with only one parameter (airspeed). For larger numbers of parameters - sometimes called multi-parametric problems—the number of samples required would grow prohibitively large. Prior work exists on specialized methods for parametric optimization, including algorithms for linear (Gal 1984; Filippi 2004), quadratic (Spjøtvold et al. 2007; Bemporad and Filippi 2003), convex (Acevedo and Salgueiro 2003; Dua and Pistikopoulos 1999), mixed integer linear (Dua and Pistikopoulos 2000), and nonlinear black-box (Hale 2005; Galvan and Malak 2015) cases. This work uses the Predictive Parametric Pareto Genetic algorithm (P3GA) introduced by Galvan and Malak (2015). P3GA can handle nonlinear black-box functions and is capable of solving single- and multi-objective parametric problems. A comparative study demonstrated that P3GA is superior to iterated application of a traditional optimization algorithm (Galvan et al. 2018). Previous implementations of P3GA focus on solving problems where the parameter values are not yet fully known but will be constant during operation (Hartl et al. 2016; Galvan et al. 2018). In the case study presented here, the parameter values are continuously changing during operation, and the structure must optimally morph in response to these changing parameters.

Optimal morphing is particularly appealing in aircraft design, where performance is critical and often costly. Morphing aero-structures are defined in this work as those that can C^1-continuously change their outer mold line (OML). Morphing expands the space of traditional aircraft control and trim methods, such as flaps and slats, to include smooth configurations with improved aerodynamic performance (Leal et al. 2018). Aviation can benefit from this technology to minimize drag (Leal et al. 2018) and noise (Maglieri et al. 2014) or to improve aircraft maneuverability (Nam et al. 2002). However, the benefits of continuous shape change are not intuitive for each flight condition and have not yet been fully explored.

Although there has been extensive work in optimizing an aircraft OML to improve overall performance, most methods have one or more of the following drawbacks: (i) no structural constraints are considered when defining geometry (Tandies and Assareh 2016; Lane and Marshall 2009; Liem et al. 2017), (ii) no analytical C^1 geometric representation exists (Liem et al. 2017; Morris et al. 2010), and/or (iii) the design is optimized for only a limited number of flight conditions (Leal et al. 2018; Tandies and Assareh 2016; Lane and Marshall 2009; Liem et al. 2017; Liu et al. 2015; Hicks and Henne 1978). Optimized configurations that do not consider (i) will result in thin airfoils that are infeasible to manufacture while drawback (ii) hinders the use of gradient-based methods or sensitivity analyses and results in high-drag OMLs. Drawback (iii) leads to designs that perform well at specific flight conditions but that underperform for all other conditions. Some have addressed (i) using thickness (Liem et al. 2017; Liu

et al. 2015) and volume (Morris et al. 2010; Hicks and Henne 1978) constraints on the OML that reproduce the inner structure restrictions. Recently, Leal and Hartl have addressed both (i) and (ii) using a structurally consistent approach based on Class/Shape Transformation (CST) equations (Leal and Hartl 2019). Additionally, parametric optimization addresses (iii) by treating flight conditions as parameters. This current work combines the CST approach with parametric optimization to yield a comprehensive approach to optimal morphing wing design. To the authors' knowledge, this article is the first application of parametric optimization to morphing wings in particular and morphing structures in general.

Section 2 is an overview of parametric optimization and the specific techniques used in this study, and Section 3 contains a description of the structurally consistent CST-based morphing wing model. Next, the morphing wing optimization problem formulation is presented (Section 4) along with results (Section 5). Finally, the parametric results are benchmarked against solutions obtained from a traditional optimization applied at samples of the parameter values (Section 6). Comparison results indicate that parametric optimization using P3GA is an effective approach for determining the optimal morphed structure across a range of operating conditions surpassing a traditional approach.

2 Parametric optimization

2.1 Theory

Parametric optimization differs from traditional methods by directly considering uncontrollable variables (i.e., parameters) during the optimization procedure. By doing so, the optimal solution is found as a function of these changing parameters. The single-objective parametric optimization problem formulation can be stated as follows (Galvan et al. 2018):

$$
\begin{aligned}
& J^*(\boldsymbol{\theta}) = \min_{\mathbf{x}} J(\mathbf{x}, \boldsymbol{\theta}) \forall \boldsymbol{\theta} \in [\boldsymbol{\theta}_{lb}, \boldsymbol{\theta}_{ub}], \\
& \text{subject to:} \\
& \quad \boldsymbol{g}(\mathbf{x}, \boldsymbol{\theta}) \leq \mathbf{0}, \\
& \quad \boldsymbol{h}(\mathbf{x}, \boldsymbol{\theta}) = \mathbf{0}, \\
& \quad \mathbf{x}_{lb} \leq \mathbf{x} \leq \mathbf{x}_{ub}, \\
& \quad \mathbf{x} \in \mathbb{R}^k, \\
& \quad \boldsymbol{\theta} \in \mathbb{R}^m,
\end{aligned}
\tag{1}
$$

where J is the scalar objective function, $\boldsymbol{\theta}$ is the parameter vector of length m, $J^*(\boldsymbol{\theta})$ is the optimal objective value as a function of the parameters (i.e., $J^*(\boldsymbol{\theta}) : \mathbb{R}^m \rightarrow \mathbb{R}$), the vector $\mathbf{x}$ is the optimization variable vector of length k, and $\boldsymbol{g}$ and $\boldsymbol{h}$ represent the inequality and equality constraints, respectively, as functions of the optimization variables and parameters. Both the optimization variables and parameters are constrained by upper bounds $(\mathbf{x}_{ub}, \boldsymbol{\theta}_{ub})$ and lower bounds $(\mathbf{x}_{lb}, \boldsymbol{\theta}_{lb})$. The vector $\mathbf{x}^*(\boldsymbol{\theta})$ represents the optimal optimization variables for any variation of the parameters (i.e., $\mathbf{x}^*(\boldsymbol{\theta}) : \mathbb{R}^m \rightarrow \mathbb{R}^k$) such that:

$$
J^*(\boldsymbol{\theta}) = J(\mathbf{x}^*(\boldsymbol{\theta}), \boldsymbol{\theta}). \tag{2}
$$

In this work, $J^*(\boldsymbol{\theta})$ is called the *performance model*, and $\mathbf{x}^*(\boldsymbol{\theta})$ is called the *optimal solution map*. This work addresses single-objective formulations; when multiple objectives are considered, $\boldsymbol{J}^*(\boldsymbol{\theta})$ is the mathematical representation of the parameterized Pareto frontier (Malak and Paredis 2010).

The performance model can be used to determine how parameters affect optimal performance and assess which parameters are most critical. The optimal solution map provides an engineer with the optimal design configuration given a vector of parameter values. In a morphing context, this optimal solution map removes the need to perform a computationally expensive optimization algorithm during operation as conditions change. Instead, the optimal solution map $\mathbf{x}^*(\boldsymbol{\theta})$ is directly used to determine the optimal morphed shape during operation under changing conditions.

In the case of morphing aircraft, optimization variables include the variables that control wing OML (i.e., shape variables) during operation, while parameters could include variables such as airspeed, angle of attack, altitude, temperature, air density, and others. In most cases, it is unlikely that a pilot will know all of these parameter values for a given flight plan at take-off, and many parameters are subject to change during flight. Using the proposed parametric optimization technique, a pilot or a controls system is always informed of all optimal lift-to-drag ratios and corresponding shape variables for a vector of parameters describing the flight condition.

2.2 Methods

The parametric optimization algorithm utilized in this work, known as P3GA (Galvan and Malak 2015), is an extension of NSGA-II (Deb et al. 2002) that handles uncontrolled and/or non-preferential parameters. Determining dominance in a parametric optimization problem is not trivial. P3GA predicts parametric dominance as a means of selecting new designs for analysis by employing a machine learning technique throughout the optimization procedure. A comprehensive explanation of P3GA and parametric dominance is given by Galvan and Malak (2015). P3GA has been successful in both numerical and engineering studies (Hartl et al. 2016; Galvan and Malak 2015). Galvan et al. (2018) concluded that P3GA performs efficiently as the number of parameters increases by assessing its performance alongside a parametric variant of NSGA-II, known as p-NSGAII. P3GA outperformed p-NSGAII in most cases considered with two parameters, and P3GA always outperformed p-NSGAII in cases considered with three or more parameters.

P3GA directly outputs the discrete configurations (i.e., set of optimization variables and corresponding parameters) found to be optimal in addition to an implicit representation of the performance model. A Gaussian-based process such as a Kriging interpolation (van Beers and Kleijnen 2004) can approximate the optimal solution map from the optimal configurations found with P3GA as demonstrated by Hartl et al. (2016). Therefore, $\hat{\mathbf{x}}^*(\boldsymbol{\theta})$ will denote the approximate optimal solution map via Kriging interpolation. For the case study herein, the DACE toolbox (Lophaven et al. 2002) is used to train $\hat{\mathbf{x}}^*(\boldsymbol{\theta})$ using the optimal designs from P3GA and a Gaussian correlation function and a quadratic regression model (see Lophaven et al. 2002 for details on training a Kriging model).

3 Camber morphing wing description

The design problem considers the cross section of an infinite wing (i.e., an airfoil) undergoing camber morphing. The CST method is used to mathematically define all generated airfoils (Leal et al. 2017). This method has been shown to accurately represent any realistic airfoil geometry with a minimum number of variables (Kulfan 2007). The CST equations are bijective; hence, two equations are necessary to fully represent the upper and lower surfaces of the airfoil. The two surfaces are denoted herein as active (lower) and passive (upper). While the passive surface is restricted to have constant length but it is free to bend, the active surface is free to both constrict and bend. This represents the case where the lower surface contains active material. The CST equations are formulated in the non-dimensional $\psi - \zeta$ domain that is related to the physically meaningful domain $x - z$ via the airfoil chord c ($\psi = x/c$ and $\zeta = y/c$) depicted in Fig. 2. The CST equations for subsonic airfoils ($N_1 = 0.5$ and $N_2 = 1$) with trailing edge thickness $\Delta\zeta_{TE}$ are as follows:

$$\zeta_A = \psi^{0.5}(1-\psi)\sum_{i=1}^{n} A_i \frac{n!}{i!(n-i)!} psi^i (1-\psi)^{n-i} + \psi\frac{\Delta\zeta_{TE}}{2}, \tag{3}$$

$$\zeta_P = \psi^{0.5}(\psi-1)\sum_{i=1}^{n} P_i \frac{n!}{i!(n-i)!} psi^i (1-\psi)^{n-i} - \psi\frac{\Delta\zeta_{TE}}{2}, \tag{4}$$

where ζ_A and ζ_P are the non-dimensional distances perpendicular to the chord to the active and passive surfaces, ψ is the non-dimensional distance along the chord ($\psi \in [0, 1]$), A_i and P_i are the shape function coefficients, and n is the order of the Bernstein polynomials.

Leal and Hartl (2019) modified the CST equations so that children airfoils (i.e., morphed configurations) can be generated from any parent airfoil (i.e., original configuration) while considering kinematic constraints related to the internal structure; thus, all of the explored designs herein are known to be physically feasible for low strains ($\leq$ 4%), even without recourse to full structural analysis. In the model it is assumed that the overall morphing structure has or maintains the following: rigid body spars, constant leading edge radius, constant passive surface length, and constant angles between spars and passive surface. The equations above can be used to describe the children and parent configurations (denoted by a superscript c and p, respectively) by varying the values of the shape coefficients. Using an owl airfoil as an example parent airfoil (Leal et al. 2018) and an internal structure consisting of five spars, a different OML can be generated at minimal computational cost (i.e., indirect calculation) that preserves the spar dimensions as shown in Fig. 2.

A system of equations is formulated by applying (3) for n spar intersections with the child active surface, located at coordinates $(\psi^c_{A,j}, \zeta^c_A(\psi^c_{A,j}))\ \forall\ j \in [1, n]$, as follows:

$$f_j = \sum_{i=0}^{n} F_{ji} A^c_i \quad \text{or} \quad \mathbf{f} = \mathbf{F}\,\mathbf{A}, \tag{5}$$

where $\mathbf{A}$ is the active shape coefficient vector (n-dimensional), $\mathbf{f}$ is the forwards restriction vector (n-dimensional)

$$f_j = \frac{2\,\zeta^c_A(\psi^c_{A,j}) + \psi^c_{A,j}\Delta\zeta^c_{TE}}{2\sqrt{\psi^c_{A,j}}(\psi^c_{A,j}-1)} - A_0(1-\psi^c_{A,j})^n, \tag{6}$$

and $\mathbf{F}$ is the forwards function matrix ($n \times n$ dimensional), given as

$$F_{ji} = \frac{n!}{i!(n-i)!}(\psi^c_{A,j})^i(1-\psi^c_{A,j})^{n-i}. \tag{7}$$

If all coordinates $(\psi^c_{A,j}, \zeta^c_A(\psi^c_{A,j}))$ can be calculated, $\mathbf{F}$ is a square tensor and invertible, and the values of the active children shape coefficients A^c_i are determined by solving the linear system of equations (5). Therefore, the only free

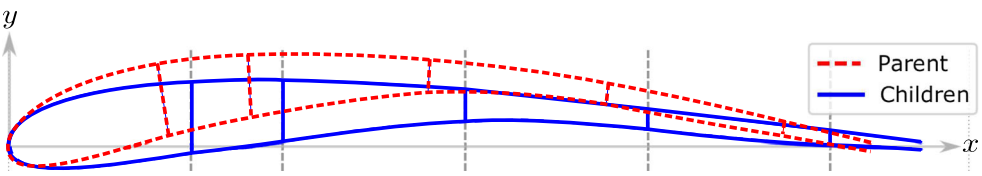

Fig. 2 Morphing airfoil example

degrees of freedom for the children configurations are the passive shape coefficients $\mathbf{P}^c$.

As detailed in Leal and Hartl (2019), a set of kinematic constraints is utilized to guarantee structural feasibility of the morphed configurations and to establish coordinates $(\psi^c_{A,j},\ \zeta^c_A(\psi^c_{A,j}))$ as a function of $\mathbf{A}^p$, $\mathbf{P}^p$, $\mathbf{P}^c$, and the locations and heights of spars. In the context of real aircraft, the parent airfoil and much of its internal structure are fixed and known. Therefore, the children airfoils are only a function of $\mathbf{P}^c$, used herein as the optimization variables. For this work, the shape coefficients of a NACA 0012 airfoil using fourth-order Bernstein polynomials are used and denoted in Table 1. A symmetric airfoil is chosen to demonstrate that morphing is effective even for an airfoil with initially no camber, even as compared with other examples of non-morphing airfoils as will be shown. The non-dimensional spar locations are also fixed at 0.1, 0.3, 0.6, and 0.8.

Since the framework (i) guarantees kinematically acceptable deformation states, (ii) only consists of linear system of kinematic equations, (iii) assumes that enough force is generated to obtain the desired strains, and (iv) strictly limits the strains generated anywhere in the morphing body to be within material limits, structural analysis is not necessary and the generation of new children configurations is greatly expedited. The framework is independent of actuator technology, but previous work has shown that shape memory alloy actuators, for example, can generate the necessary strains for a camber morphing wing (Leal et al. 2018).

4 Parametric formulation of a morphing aerostructure design problem

The optimal morphing aerostructure problem can be formulated as a multi-parametric optimization problem, where the single objective is to maximize the lift-to-drag ratio. This ratio is determined by calculating the coefficients of lift and drag using XFOIL (Drela 2001), a subsonic panel-method aerodynamic solver. The operational parameters considered are angle of attack α, airspeed V, and altitude H, all of which vary during flight. For this work, the optimization variables are the shape coefficients of the child (morphed) airfoil P^c_i for $i = [1, 2, 3, 4]$, where each coefficient is spatially predominant in a different chordwise location. Together, the four shape coefficients define the airfoil shape (see Table 1 for parent shape coefficients $\mathbf{P}^p$). P^c_1 and P^c_4 dominate respectively the leading and trailing edges, while P^c_2 and P^c_3 are most relevant for intermediate chordwise coordinates. All other aspects of the problem, such as the initial NACA 0012 shape and spar locations are held constant to allow clarity of presentation. CST equations of order $n = 4$ are utilized based on a convergence study performed by Leal and Hartl (2019). Depending on the requirements of the design exploration, n can be increased to allow more subtle topological manipulations and structural constraints (e.g., spars).

Table 1 Shape coefficients for parent (reference) NACA 0012 airfoil considered in this work from which all morphed configurations are generated

P^p_0	P^p_1	P^p_2	P^p_3	P^p_4
0.1828	0.1179	0.2079	0.0850	0.1874
A^p_0	A^p_1	A^p_2	A^p_3	A^p_4
0.1702	0.1528	0.1592	0.1195	0.1651

The mathematical problem formulation is thus:

$$J^*(\alpha, V, H) = \max_{\mathbf{P}^c} J(\mathbf{P}^c; \alpha, V, H),$$

Subject to:

$$\begin{aligned} &\mathbf{P}^c \in \mathbb{P}, \\ &\begin{bmatrix} 0^\circ \\ 20\text{m/s} \\ 5000\text{ft} \end{bmatrix} \leq \begin{bmatrix} \alpha \\ V \\ H \end{bmatrix} \leq \begin{bmatrix} 12^\circ \\ 65\text{m/s} \\ 40000\text{ft} \end{bmatrix}, \end{aligned} \tag{8}$$

where the objective function J represents the lift-to-drag ratio, $J^*(\alpha, V, H)$ represents the maximum lift-to-drag ratio as a function of the parameters, $\mathbf{x} = \mathbf{P}^c$, and $\boldsymbol{\theta} = [\alpha, V, H]^T$.

To prevent generating shapes that either are unreasonable or cannot be accurately studied with XFOIL, the shape coefficients are conservatively constrained based on feasible, existing airfoil shapes. This feasible set is denoted $\mathbb{P}$. To quantify this constraint, 1636 shape coefficient vectors are calculated for all the airfoils contained in a given database (Selig 1995). A thorough investigation of this four-dimensional data revealed that the feasible space would not be easily constrained via linear constraints. As shown by Malak and Paredis (2010), a Support Vector Domain Description (SVDD) can be trained to fit the data and provide a single, nonlinear constraint. This SVDD is a one-class classifier that, once trained, predicts whether a new data point lies inside or outside of the class (Tax and Duin 1999). In this case, the class being trained is that of feasible airfoil shapes.

5 Results

Since the solution of a single-objective three-parameter problem cannot be readily visualized in 4-D space, results are herein presented in two phases. Section 5.1 presents a two-parameter subset of the solution where altitude is fixed at 10,000 ft while angle of attack and airspeed are still

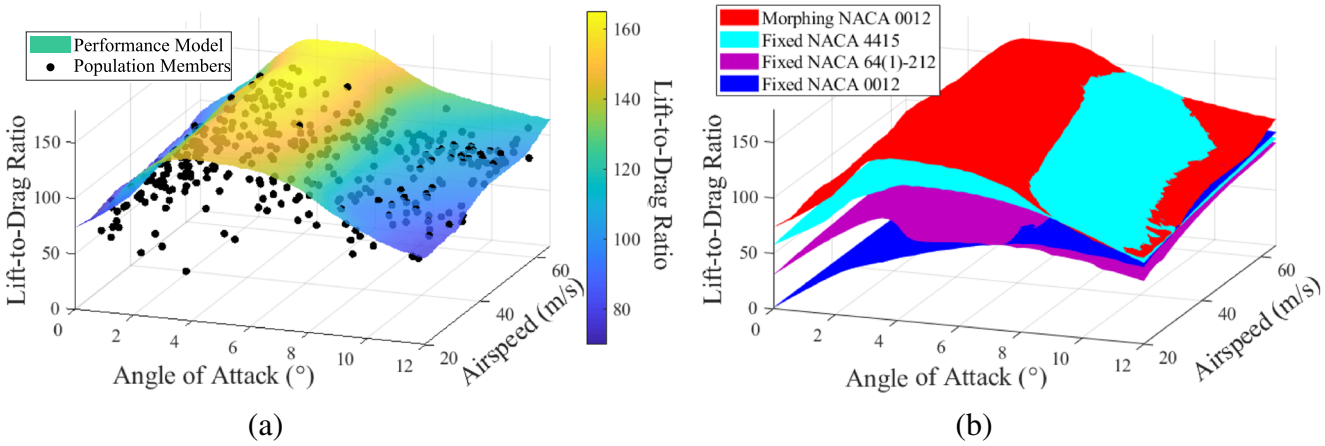

Fig. 3 Results considering altitude held constant at 10,000 ft. **a** Population of structurally feasible morphed designs projected into this 3-D domain and lift-to-drag ratios of optimal performance across changing flight conditions. **b** Comparison between the performance of the morphing NACA 0012 configurations and that of a fixed NACA 0012, a fixed NACA 4415 and a fixed NACA 64(1)-212

treated as parameters. Then, Section 5.2 conveys the full, three-parameter solution.

5.1 Two-parameter problem

Considering a fixed altitude of 10,000 ft, the performance model over changing angle of attack and airspeed is illustrated by the surface in Fig. 3a. Depending on the parameter values, lift-to-drag ratios of up to 169 are achieved. Overall, the optimal lift-to-drag ratio monotonically increases as airspeed V increases. An increase of angle of attack for smaller angles ($\alpha \leq 5°$) results in an increase of this objective. However, for higher angles of attack ($\alpha > 5°$), the lift-to-drag ratio decreases because of sensitivity to stalling (Drela 2001). Figure 3b shows a comparison between the performance for the camber *morphing* NACA 0012 and three *fixed* airfoils for the same flight conditions (including the fixed NACA 0012). The benefits of using a morphing

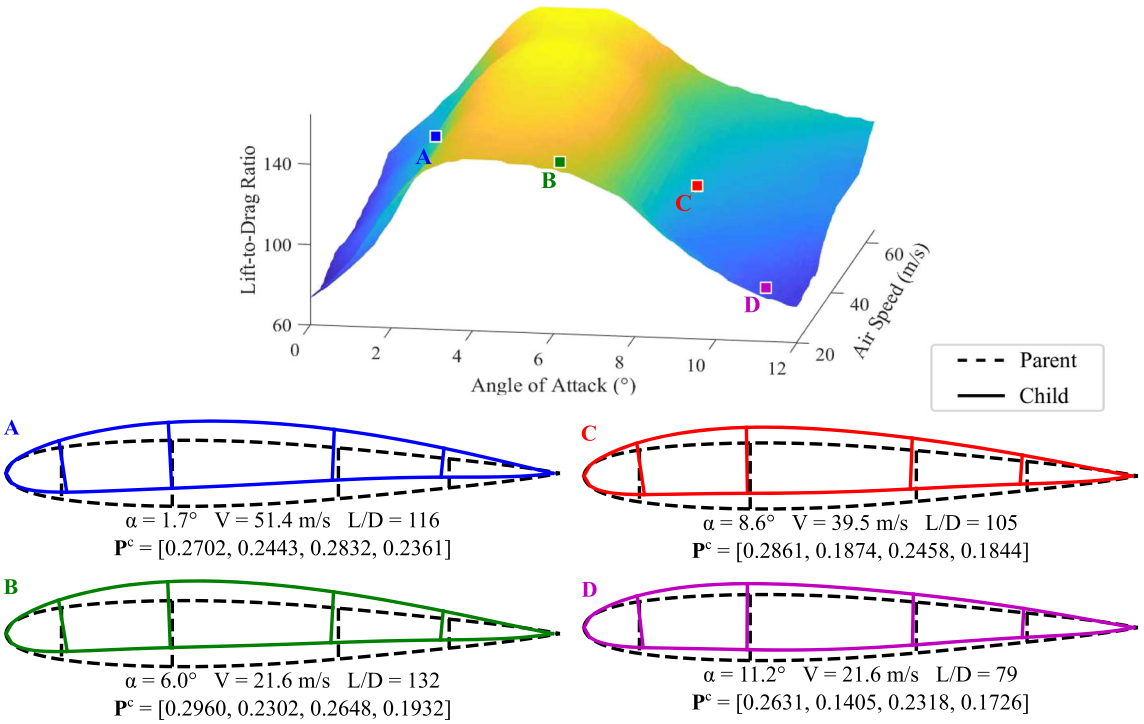

Fig. 4 Four structurally consistent morphed configurations from the optimal solution map for low (design **A**), medium (design **B**), and high (designs **C** and **D**) angles of attack and their relation to the performance model are depicted along with airfoil shape coefficients, designed flight condition, and lift-to-drag ratio

airfoil are apparent at smaller angles of attack where significant increases in achievable lift-to-drag ratios are obtained. For higher angles of attack, the morphing optimization seems to be less relevant for this parent airfoil. Although there is one region ($\alpha \in (7°, 11°)$) where the fixed NACA 4415 dominates, the morphing NACA 0012 appears to outperform all considered fixed airfoils for the majority of these flight parameters. The maximum benefit seen by the fixed NACA 4415 over the morphing NACA 0012 is an increase of 18.8 of the lift-to-drag ratio. However, the lift-to-drag ratio of the morphing NACA 0012 is on average 9 points higher than that of the fixed NACA 4415. Additionally, the morphing NACA 0012 always outperforms the fixed NACA 4415 for the lower angles of attack that airplanes more commonly operate. This result shows that the morphing NACA 0012 is physically unable to match the performance of the NACA 4415 shape due to the structurally consistent constraints. This gives evidence to support analyzing a *morphing* NACA 4415 concept especially when looking at higher angle of attack applications.

The optimal morphed configuration clearly changes with flight condition, but four distinct families can be clustered based on their topology (Arthur and Vassilvitskii 2007). Figure 4 illustrates how the performance model and optimal solution map can be used together to display these four families of airfoils. The depicted airfoils are the cluster centers (Arthur and Vassilvitskii 2007) for each family of solutions. At lower angles of attack ($\alpha < 4°$), the morphed configurations (design A) are similar to traditional high-lift airfoils (Abbott and Doenhoff 1959). As angle of attack increases ($4° \leq \alpha < 7°$), the maximum camber location tends towards the leading edge, resulting in configurations (design B) similar to avian airfoils (Bansmer et al. 2012). As angle of attack continues to increase ($7° \leq \alpha < 9°$), the high camber at the front of the airfoil decreases, leading to traditional airfoil shapes (design C). At the highest angles of attack, camber is decreased to delay boundary layer separation, leading to unorthodox designs (design D) known as reflexed airfoils (Jacobs and Pinkerson 1936; Pankonien et al. 2016). Each of the identified designs is not acceptable

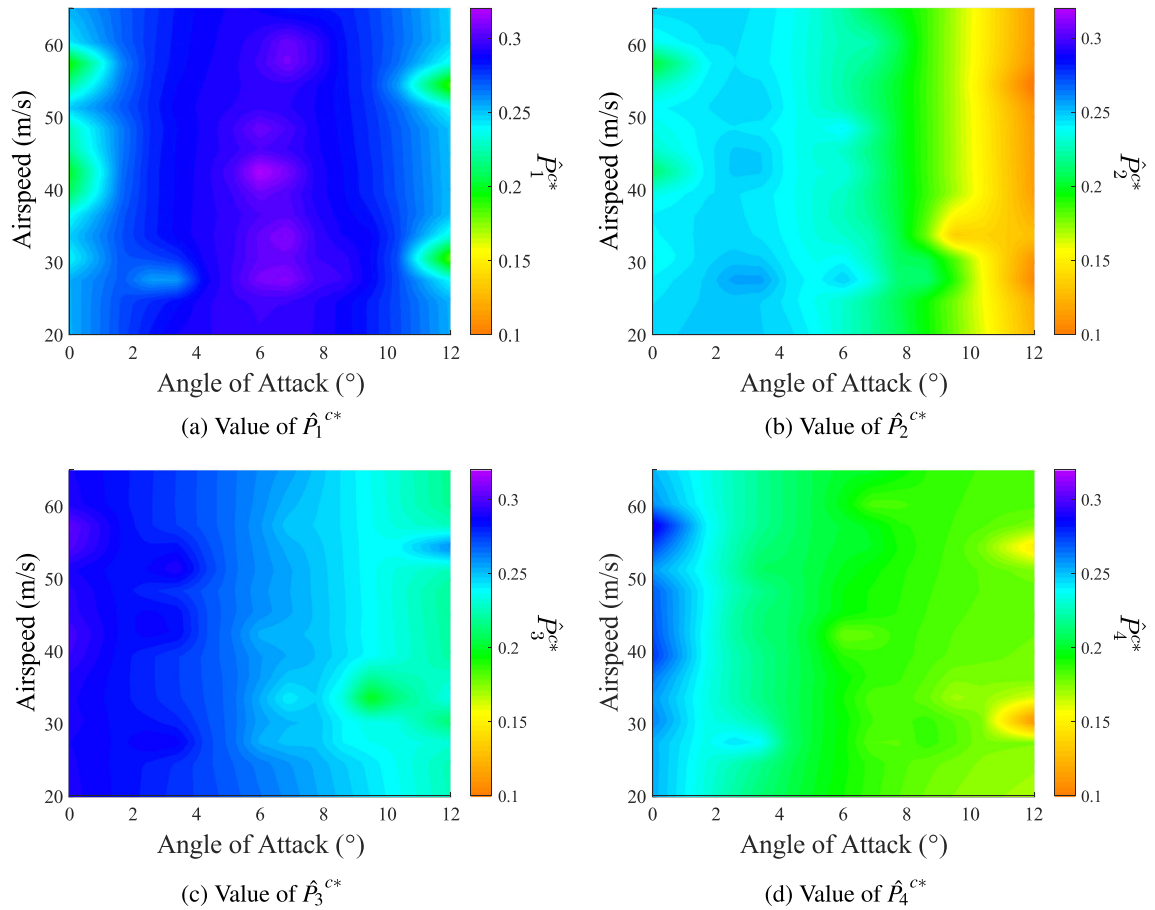

(a) Value of $\hat{P}_1^{c*}$ (b) Value of $\hat{P}_2^{c*}$

(c) Value of $\hat{P}_3^{c*}$ (d) Value of $\hat{P}_4^{c*}$

Fig. 5 Approximate optimal solution map providing the value of each shape coefficient for the camber morphing NACA 0012 when altitude is fixed at 10,000 ft. Such a map could be used to schedule a controller such that morphing structures automatically adapt during operation. **a** Value of $\hat{P}_1^{c*}$. **b** Value of $\hat{P}_2^{c*}$. **c** Value of $\hat{P}_3^{c*}$. **d** Value of $\hat{P}_4^{c*}$

for all flight conditions, but is viable as one of many states of a morphing airfoil.

Figure 5 illustrates the optimal solution map approximation, $\hat{\mathbf{P}}^{c*}(\alpha, V, H)$, for each shape coefficient over the subset of the parameter space where $H = 10{,}000$ ft. For lower angles of attack ($\alpha < 7°$), $\hat{P}_1^{c*}$ increases, $\hat{P}_2^{c*}$ fluctuates near its highest value, and $\hat{P}_3^{c*}$ and $\hat{P}_4^{c*}$ decrease to augment camber and relocate the maximum camber location towards the leading edge. At higher angles of attack ($\alpha \geq 9°$), all shape coefficients decrease to curtail camber, generating children configurations similar to the parent airfoil.

5.2 Three-parameter problem

Although the four-dimensional performance model (three parameters and one objective) can be difficult to visualize directly, depicting multiple two-dimensional subsets for a fixed aircraft speed and altitude is enlightening (Fig. 6). Figure 6a displays the two-dimensional solution subsets at four different airspeeds while fixing altitude at 20,000 ft. Likewise, Fig. 6b displays the two-dimensional solution subsets at four different altitudes with airspeed fixed at 35 m/s.

Visualizing these reduced subsets of the four-dimensional performance model reiterates the trend seen in the two-parameter solution, and also elucidates how this model is affected by altitude variations. The lift-to-drag ratio monotonically increases as airspeed increases while the effect of angle of attack is not as straightforward. Angle of attack continues to maximize the lift-to-drag ratio near 5°, but variations in altitude change this peak slightly. While the curves for 10,000 and 20,000 ft are similar, the performance begins to decrease more rapidly for altitudes of 30,000

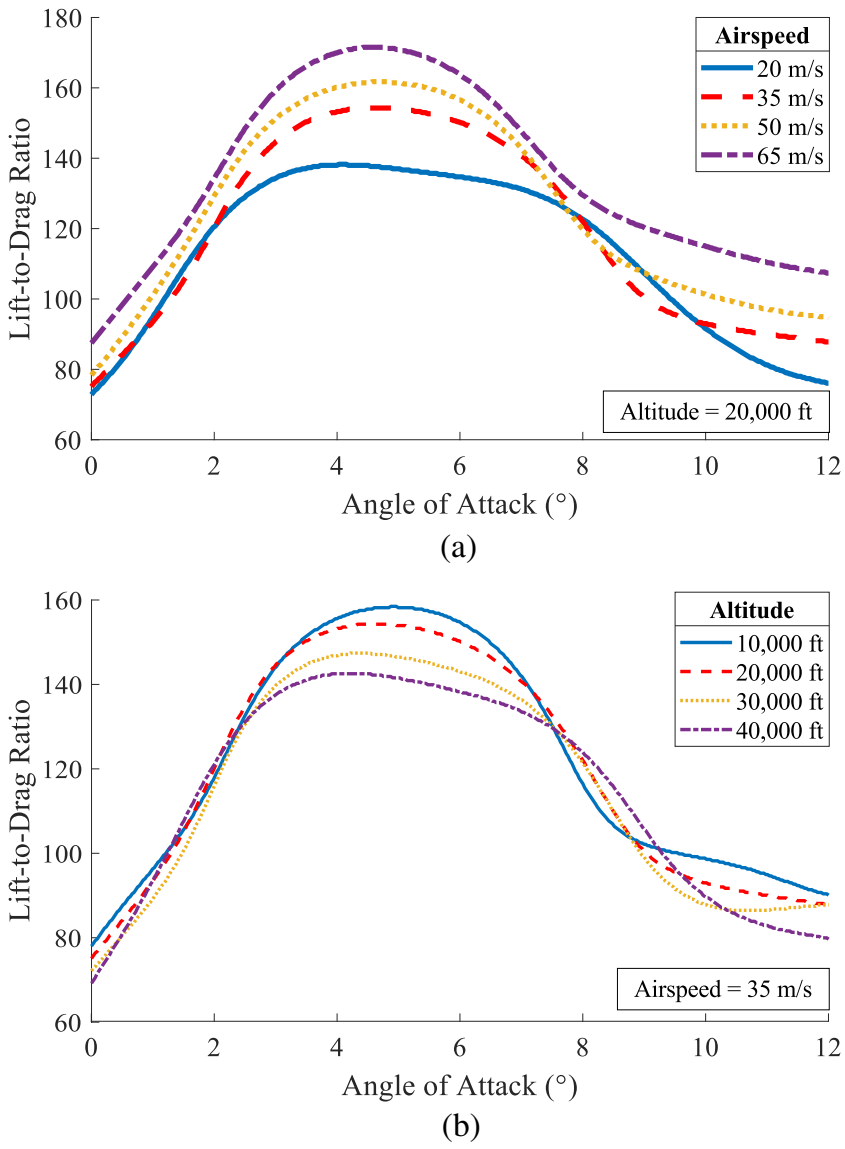

Fig. 6 Two-dimensional subsets of the four-dimensional performance model for the morphing airfoil: **a** sections of this model where altitude is fixed at 20,000 ft and airspeed is sampled at 20, 35, 50, and 65 m/s; **b** sections of the same model fixing airspeed at 35 m/s and aircraft altitude at 10, 20, 30, and 40 thousand feet

and 40,000 ft. This is the expected response as air density decreases at higher altitudes, leading to varying Reynolds numbers (i.e., different flow regimes). Note that the performance model somewhat deviates from these trends when the angle of attack is near 2° and 8°, which may be an artifact of aerodynamic instabilities in these regions.

Figure 7 displays the shape coefficient values (cf. Fig. 5) with angle of attack and altitude featured on the horizontal and vertical axes, respectively, and airspeed fixed at 35 m/s. The subset of the optimal solution map represented by Fig. 7 shows that altitude has very little effect on the optimal morphed airfoil shapes, even though the optimal *performance* of these airfoils is affected (cf. Fig. 6). In the interest of brevity, only a small subset of the full optimal solution map is visualized.

With respect to computational cost, the runtime for the full parametric optimization loop that solves (8) for all three parameters using P3GA is approximately 117 h for 400 generations with a population size of 150 individuals (Intel i7 core processor with 8 GB of RAM). The majority of this runtime is spent evaluating the objective function via XFOIL, which requires 6 to 20 s depending on the aerodynamic complexity. In this case, the computational cost of the methods used within P3GA (i.e., machine learning) are negligible compared with objective function cost.

6 Benchmarking

To quantify any errors in the performance model, its output is compared with that from multiple executions of a traditional genetic algorithm (each with a different set of fixed parameter values). Sixty-four parameter combinations selected via a Latin Hypercube sampling (LHS) for the morphing NACA 0012 parent shape are considered and represent 64 single-objective individual optimizations to obtain the maximum lift-to-drag ratio, $J^\flat$, and optimal shape coefficients, $P_i^{c\flat}$, using the built-in GA in MATLAB (2017b). Default algorithmic settings are used, and the results are taken as truth solutions as convergence to within a small tolerance occurs. Note that the solutions to the 64 genetic optimizers required 1344 h in total, though direct comparison

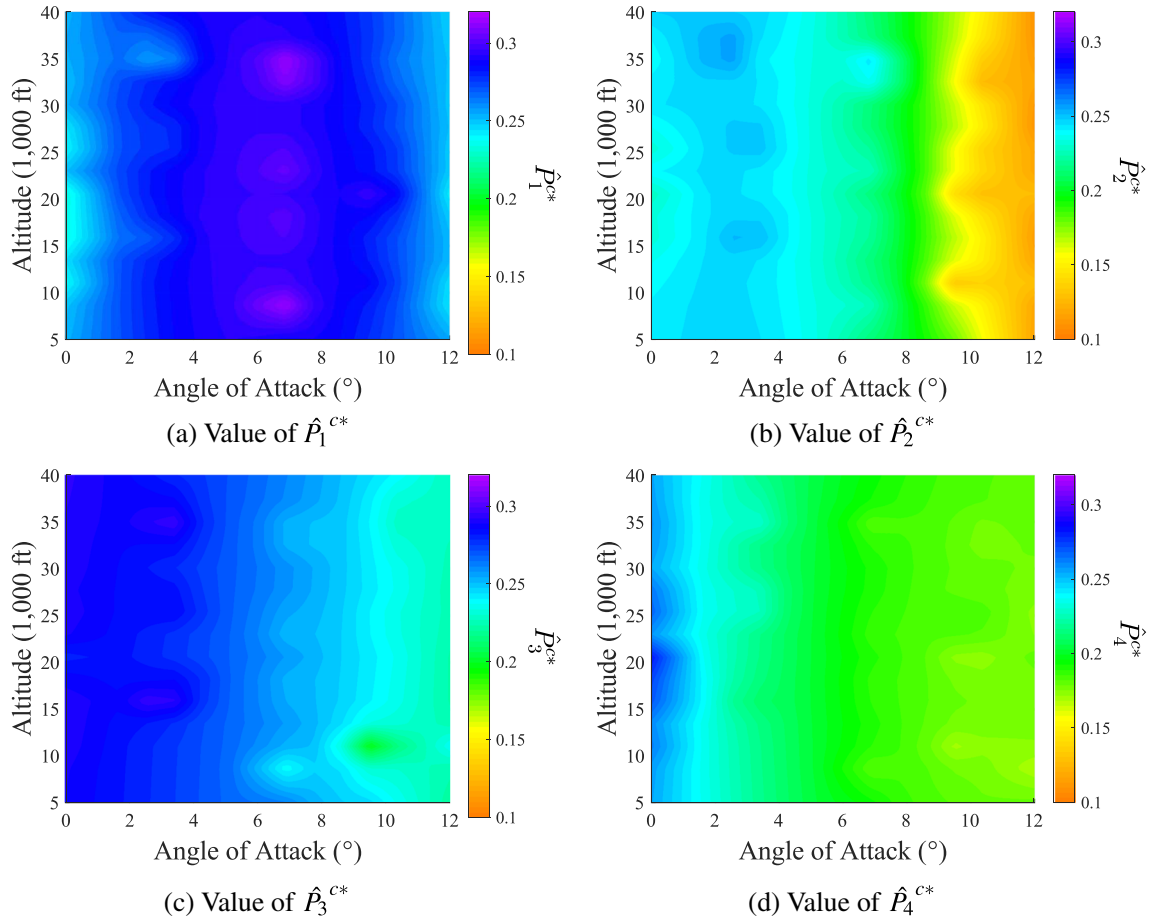

(a) Value of $\hat{P}_1^{c*}$ (b) Value of $\hat{P}_2^{c*}$

(c) Value of $\hat{P}_3^{c*}$ (d) Value of $\hat{P}_4^{c*}$

Fig. 7 Approximate optimal solution map providing the value of each shape coefficient for the camber morphing NACA 0012 when airspeed is fixed at 35 m/s. **a** $\hat{P}_1^{c*}$. **b** $\hat{P}_2^{c*}$. **c** $\hat{P}_3^{c*}$. **d** $\hat{P}_4^{c*}$

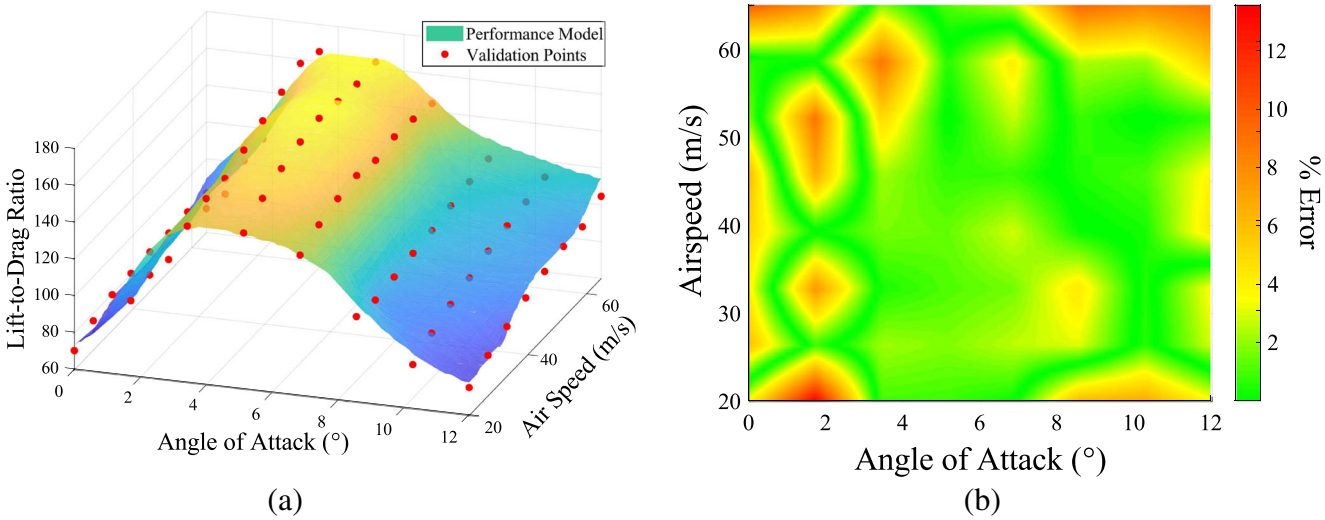

Fig. 8 Results of parametric optimization via P3GA contrasted with the results of the traditional genetic algorithm (Goldberg and Holland 1988): **a** the performance model (surface) as compared with the 8×8 grid of traditional optimization solutions (points), **b** percent error between the performance model and validation points as calculated via (9)

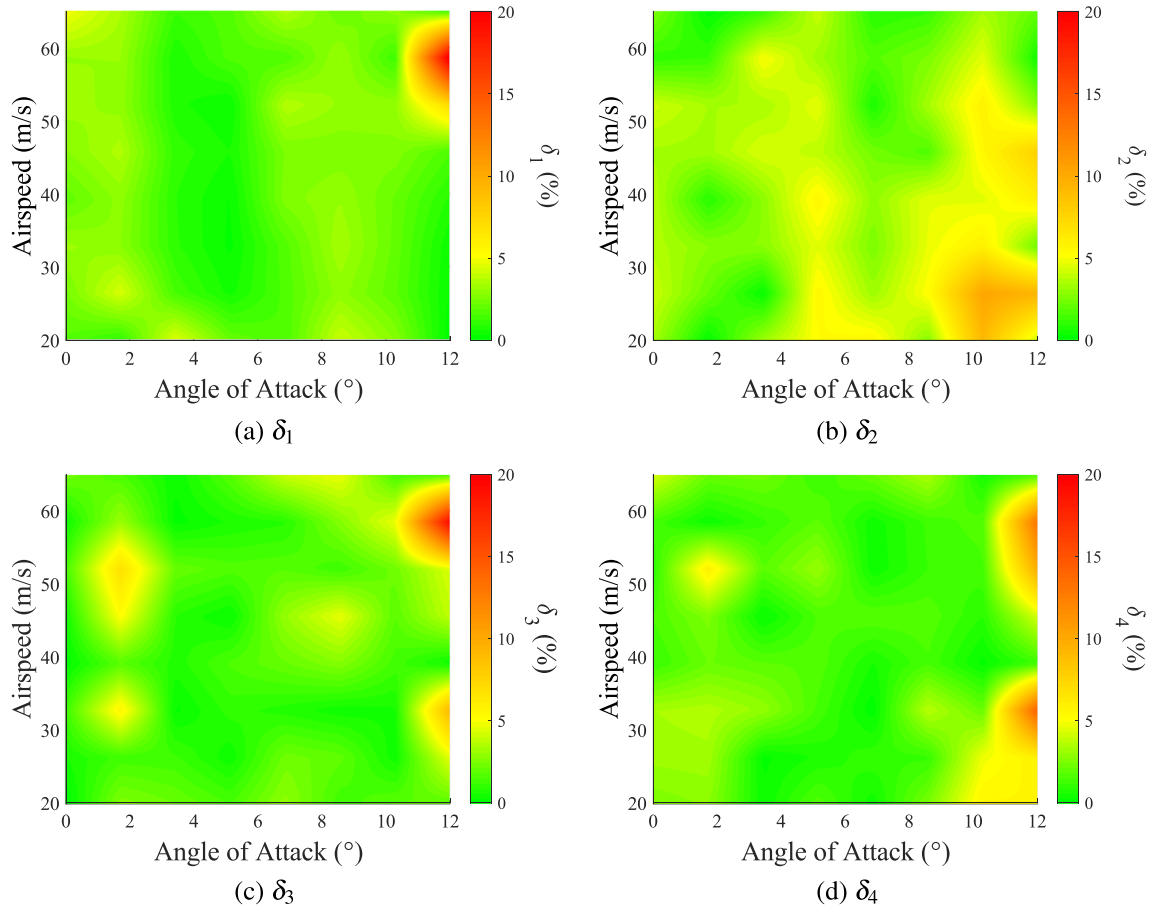

Fig. 9 Difference between the results of the optimal solution map and the traditional genetic algorithm (Goldberg and Holland 1988) from the four optimization variables (P_1^c, P_2^c, P_3^c, and P_4^c) using (10) for the two-parameter subset where altitude is fixed at 10,000 ft. **a** δ_1. **b** δ_2. **c** δ_3. **d** δ_4

with P3GA's runtime of 117 h is inconclusive since P3GA did not enforce any stopping criteria beyond the maximum number of generations. All optimizations performed in this study (via P3GA and a traditional genetic algorithm) are done using a quad-core computer with a 2.93 GHz Intel i7-870 processor and 8 GB of RAM. Additionally, both P3GA and genetic algorithms in general are highly parallelizable. Therefore, all presented results are generated from four parallel processes to evaluate the population members among each generation of both P3GA and the benchmarking genetic algorithm. The error of the performance model is quantified using (9).

$$\text{Error}\,(\boldsymbol{\theta}) = \frac{\left|J^{*}(\boldsymbol{\theta}) - J^{\flat}(\boldsymbol{\theta})\right|}{\left|J^{\flat}(\boldsymbol{\theta})\right|} \tag{9}$$

The average and standard deviation of the error in performance among the 64 fixed parameter sites considered are 2.85% and 3.30%, respectively. To provide a graphical representation, another study is performed where a two-parameter subset of the full solution is explored to allow for visualization in three dimensions (two parameters and one objective). Fixing the altitude parameter at 10,000 ft, an 8×8 grid of combinations of angle of attack and airspeed are chosen to run a total of 64 *additional* iterations of a traditional genetic algorithm. These 64 combinations are plotted in red over the performance model in Fig. 8a for this fixed altitude. P3GA is able to represent the trends of the true solution very well. The errors (defined in (9)) of this subset are largely within 5%, as shown in Fig. 8b.

Finally, the full optimal solution map from parametric optimization is benchmarked against the discrete optimal configurations for the original 64 points in parameter space via LHS. The differences between the shape coefficients from the optimal solution map and those from fixed-parameter optimizations are given by:

$$\delta_i\,(\boldsymbol{\theta}) = \frac{\left|\hat{P}_i^{\,c*}(\boldsymbol{\theta}) - P_i^{c\flat}(\boldsymbol{\theta})\right|}{x_{ub,i} - x_{lb,i}} \forall i \in [1, 2, 3, 4]\,, \tag{10}$$

where $\hat{P}_i^{\,c*}(\boldsymbol{\theta})$ is the optimal ith shape coefficient predicted by the Kriging model of the optimal solution map and $P_i^{c\flat}(\boldsymbol{\theta})$ is the optimal ith shape coefficient predicted by the fixed-parameter optimizations via a common GA (Goldberg and Holland 1988). This difference is normalized by the bounds of shape coefficients which are determined by the 1636 feasible airfoils and introduced via the nonlinear constraint. All shape coefficients are allowed to vary from ± 0.5; thus, the denominator of (10) equals 1. The average differences for each of the four shape coefficients are 2.38%, 3.48%, 1.85%, and 2.34%, respectively. To allow for visualization of these differences, a subset of the optimal solution map at $H = 10,000$ ft is visualized for each shape coefficient based on the same 8×8 grid over angle of attack and airspeed from before (Fig. 9). This agreement gives evidence to support the use of parametric optimization in a morphing context as a preliminary step in calculating the optimal shape variables for many sets of external conditions.

7 Conclusion

This work shows the potential of parametric optimization as applied to the design of a morphing structure. P3GA is shown to be an effective tool for optimizing a flight performance objective function over a range of parameters, making it a useful method for optimizing morphing structures. The results of parametric optimization using P3GA are found to be within a reasonable error tolerance as compared with traditional methods, with the advantage of capturing a more detailed understanding of the parameter space at a reduced computational cost. This accuracy, coupled with the decreased runtime compared with traditional methods (Galvan et al. 2018), supports the use of parametric optimization for solving morphing problems over traditional optimization methods. Visualizing the parametric solutions (performance model and optimal solution map), even when the solution dimensionality is greater than three, is demonstrated by viewing subsets. The full performance model is found to have an average error of approximately 2.85%, and the optimal solution map has average errors of less than 3.5% for each of the four optimization variables (shape coefficients). The two-parameter performance model describing the morphing NACA 0012 lift-to-drag ratios compared with those from non-morphing baseline designs motivates morphing technologies and shows that morphing airfoils can drastically improve wing performance and achieve similar or better performance across changing operational conditions than fixed, specialized airfoils. Future work will consider (i) other parent airfoil configurations (shape and number/spacing of spars), (ii) exploring other benefits of parametric optimization when designing and operating morphing structures, and (iii) solving the optimal solution map for cases where approximation via an interpolation method is not valid. These studies will serve to further strengthen the case for using parametric optimization and the associated methodologies in the design and operation of morphing technologies.

Funding information This work is supported by the NASA *University Leadership Initiative* (ULI) program under federal award number NNX17AJ96A, titled Adaptive Aerostructures for Revolutionary Civil Supersonic Transportation.

Compliance with Ethical Standards

Conflict of interest The authors declare that they have no conflict of interest.

Replication of results Although the results presented are obtained from stochastic methods, the same type of results could be replicated. The morphing airfoil framework is publicly available on GitHub (https://github.com/leal26/AeroPy), and P3GA can be made available upon request.

References

Abbott IH, Doenhoff AEV (1959) Theory of wing sections, including a summary of airfoil data. Courier Corporation, google-books-iD: DPZYUGNyuboC

Acevedo J, Salgueiro M (2003) An efficient algorithm for convex multiparametric nonlinear programming problems. Ind Eng Chem Res 42(23):5883–5890. https://doi.org/10.1021/ie0301278

Arthur D, Vassilvitskii S (2007) k-means++: the advantages of careful seeding. In: Proceedings of the eighteenth annual ACM-SIAM symposium on discrete algorithms, society for industrial and applied mathematics, pp 1027–1035

Bansmer S, Buchmann N, Radespiel R, Unger R, Haupt M, Horst P, Heinrich R (2012) Aerodynamics and structural mechanics of flapping flight with elastic and stiff wings. In: Tropea C, Bleckmann H (eds) Nature-inspired fluid mechanics, vol 119. Springer, Berlin, pp 331–354. https://doi.org/10.1007/978-3-642-28302-420

Bemporad A, Filippi C (2003) Suboptimal explicit receding horizon control via approximate multiparametric quadratic programming. J Optim Theory Appl 117(1):9–38. https://doi.org/10.1023/A:1023696221899

Deb K, Pratap A, Agarwal S, Meyarivan T (2002) A fast and elitist multiobjective genetic algorithm: NSGA-II. IEEE T Evolut Comput 6(2):182–197

Drela M (2001) XFOIL 6.9 user primers. MIT AERO and Astro Harold Youngren, Aerocraft, Incl

Dua V, Pistikopoulos EN (1999) Algorithms for the solution of multiparametric mixed-integer nonlinear optimization problems. Ind Eng Chem Res 38(10):3976–3987. https://doi.org/10.1021/ie980792u

Dua V, Pistikopoulos EN (2000) An algorithm for the solution of multiparametric mixed integer linear programming problems, p 17

Fiacco AV (1976) Sensitivity analysis for nonlinear programming using penalty methods. Math Program 10(1):287–311. https://doi.org/10.1007/BF01580677

Filippi C (2004) An algorithm for approximate multiparametric linear programming. J Optimiz Theory App 120(1):73–95. https://doi.org/10.1023/B:JOTA.0000012733.44020.54

Gal T (1984) Linear parametric programming—a brief survey. Springer, Berlin, pp 43–68. https://doi.org/10.1007/BFb0121210

Galvan E, Malak RJ (2015) P3ga: an algorithm for technology characterization. J Mech Des 137(1):011401

Galvan E, Malak RJ, Hartl DJ, Baur JW (2018) Performance assessment of a multi-objective parametric optimization algorithm with application to a multi-physical engineering system. Struct Multidiscip Optim 58(2):489–509. https://doi.org/10.1007/s00158-018-1902-x

Gamboa P, Vale J, Lau FJP, Suleman A (2009) Optimization of a morphing wing based on coupled aerodynamic and structural constraints, vol 47. https://doi.org/10.2514/1.39016

Goldberg DE, Holland JH (1988) Genetic algorithms and machine learning. Mach Learn 3(2):95–99

Hale ET (2005) Numerical methods for d-parametric nonlinear programming with chemical process control and optimization applications. Chemical Engineering Department, University of Texas. Austin, TX

Hartl DJ, Galvan E, Malak RJ, Baur JW (2016) Parameterized design optimization of a magnetohydrodynamic liquid metal active cooling concept. J Mech Des 138(3):031402

Hicks RM, Henne PA (1978) Wing design by numerical optimization. J Aircr 15(7):407–412. https://doi.org/10.2514/3.58379

Jacobs E, Pinkerson R (1936) Tests in the variable-density wind tunnel of related airfoils having the maximum camber unusually far forward. NACA-TR-537, U.S. environmental protection agency available through the National Technical Information Service, Springfield, VA. Langley Field, VA, United States

Kulfan B (2007) Recent extensions and applications of the "CST" universal parametric geometry representation method. In: 7th AIAA aviation technology, integration and operations conference (ATIO). American Institute of Aeronautics and Astronautics. https://doi.org/10.2514/6.2007-7709

Lane K, Marshall D (2009) A surface parameterization method for airfoil optimization and high lift 2d geometries utilizing the cst methodology. American Institute of Aeronautics and Astronautics. https://doi.org/10.2514/6.2009-1461

Leal PB, Stroud H, Sheahan E, Cabral M, Hartl DJ (2018) Skin-based camber morphing utilizing shape memory alloy composite actuators in a wind tunnel environment. American Institute of Aeronautics and Astronautics. https://doi.org/10.2514/6.2018-0799

Leal PBC, Hartl DJ (2019) Structurally consistent class/shape transformation equations for morphing airfoils. J Aircr 56(2):505–516. https://doi.org/10.2514/1.C035025

Leal PBC, Patterson R, Hartl DJ (2017) Design optimization toward a shape memory alloy-based bio-inspired morphing wing. https://doi.org/10.2514/6.2017-0054

Leal PBC, Savi MA, Hartl DJ (2018) Aero-structural optimization of shape memory alloy-based wing morphing via a class/shape transformation approach. P I Mech Eng G-J Aer 232(15):2745–2759. https://doi.org/10.1177/0954410017716193

Liem RP, Martins JR, Kenway GK (2017) Expected drag minimization for aerodynamic design optimization based on aircraft operational data. Aerosp Sci Technol 63:344–362. https://doi.org/10.1016/j.ast.2017.01.006

Liu Y, Yang C, Song X (2015) An airfoil parameterization method for the representation and optimization of wind turbine special airfoil. J Therm Sci 24(2):99–108. https://doi.org/10.1007/s11630-015-0761-7

Lophaven SN, Nielsen HB, Sondergaard J (2002) Dace - a Matlab kriging toolbox, Version 2.0. Technical Report No IMM-TR-2002-12

Maglieri DJ, Bobbitt PJ, Plotkin KJ, Shepherd KP, Coen PG, Richwine DM (2014) Sonic boom: six decades of research. NASA Langley Research Center, Hampton, Virginia, United States, NASA SP-2014-622

Malak RJ, Paredis CJJ (2010) Using support vector machines to formalize the valid input domain of predictive models in systems design problems. J Mech Des 132(10):101001. https://doi.org/10.1115/1.4002151

MATLAB (2017b) MATLAB user manual R2017b

Morris AM, Allen CB, Rendall TCS (2010) High-fidelity aerodynamic shape optimization of modern transport wing using efficient hierarchical parameterization. Int J Numer Methods Fluids 63(3):297–312. https://doi.org/10.1002/fld.2067

Nam C, Chattopadhyay A, Kim Y (2002) Application of shape memory alloy (SMA) spars for aircraft maneuver enhancement. In: SPIE's 9th annual international symposium on smart structures and materials, international society for optics and photonics, pp 226–236

Pankonien AM, Gamble L, Faria C, Inman DJ (2016) Synergistic smart morphing aileron: capabilites identification. American institute of aeronautics and astronautics. https://doi.org/10.2514/6.2016-1570

Pistikopoulos EN, Dua V, Bozinis NA, Bemporad A, Morari M (2004) On-line optimization via off-line parametric optimization tools. Comput Chem Eng 24(2-7):183–188

Selig M (1995) Summary of low speed airfoil data. SoarTech publications

Spiegel M, Subrahmanyam A (2015) Informed speculation and hedging in a noncompetitive securities market. Rev Financ Stud 5(2):307–329. https://doi.org/10.1093/rfs/5.2.307. http://oup.prod.sis.lan/rfs/article-pdf/5/2/307/24417338/050307.pdf

Spjøtvold J, Tøndel P, Johansen TA (2007) Continuous selection and unique polyhedral representation of solutions to convex parametric quadratic programs. J Optim Theory Appl 134(2):177–189. https://doi.org/10.1007/s10957-007-9215-z

Tandies E, Assareh E (2016) Inverse design of airfoils via an intelligent hybrid optimization technique. Eng Comput 33(3):361–374. https://doi.org/10.1007/s00366-016-0478-6

Tax DM, Duin RP (1999) Support vector domain description. Pattern Recogn Lett 20(11-13):1191–1199. https://doi.org/10.1016/S0167-8655(99)00087-2

van Beers WCM, Kleijnen JPC (2004) Kriging interpolation in simulation: a survey. In: Proceedings of the 2004 winter simulation conference, vol 1, p 121. https://doi.org/10.1109/WSC.2004.1371308

Wang Y, Seki H, Ohyama S, Akamatsu K, Ogawa M, Ohshima M (2000) Optimal grade transition control for polymerization reactors, vol 24. https://doi.org/10.1016/S0098-1354(00)00550-0

Affiliations

Jonathan M. Weaver-Rosen[1] · Pedro B. C. Leal[2] · Darren J. Hartl[2] · Richard J. Malak Jr.[1]

Jonathan M. Weaver-Rosen
jonr23@tamu.edu

Pedro B. C. Leal
leal26@tamu.edu

Darren J. Hartl
darren.hartl@tamu.edu

[1] Department of Mechanical Engineering, Texas A&M University, College Station, TX, 77843, USA

[2] Department of Aerospace Engineering, Texas A&M University, College Station, TX, 77843, USA